

# Supporting Information

## Novel enhancement of refrigeration efficiency by strain memory effect in FeRh/PMN-PT heterostructures

Kaiming Qiao<sup>a,b</sup>, Fengxia Hu<sup>a,b,c,\*</sup>, Yao Liu<sup>a,b</sup>, Jia Li<sup>a,b</sup>, Hao Kuang<sup>a,b</sup>, Hongrui Zhang<sup>a,b</sup>,  
Wenhui Liang<sup>a,b</sup>, Jing Wang<sup>a,b,d,\*</sup>, Jirong Sun<sup>a,b,c</sup>, and Baogen Shen<sup>a,b,c,\*</sup>

<sup>a</sup>Beijing National Laboratory for Condensed Matter Physics & State Key Laboratory of Magnetism, Institute of Physics, Chinese Academy of Sciences, Beijing 100190, P. R. China;

<sup>b</sup>School of Physical Sciences, University of Chinese Academy of Sciences, Beijing 100049, P. R. China

<sup>c</sup>Songshan Lake Materials Laboratory, Dongguan, Guangdong 523808, P. R. China

<sup>d</sup>Fujian Institute of Innovation, Chinese Academy of Sciences, Fuzhou, Fujian 350108, P. R. China

\*Corresponding author

E-mail: [fxhu@iphy.ac.cn](mailto:fxhu@iphy.ac.cn); [wangjing@iphy.ac.cn](mailto:wangjing@iphy.ac.cn); [shenbg@iphy.ac.cn](mailto:shenbg@iphy.ac.cn)

### S1. Schematic $M$ - $E$ curves for FM/FE heterostructures with different types of FE

substrates.

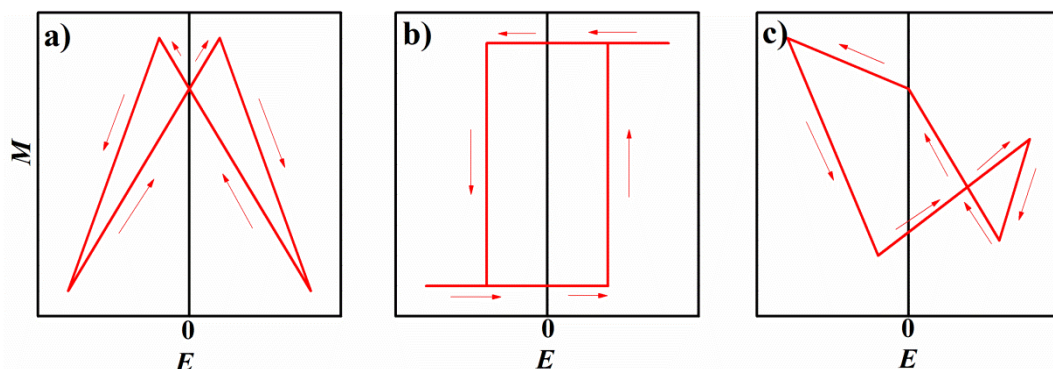


**Figure S1.** Schematic  $M$ - $E$  curves for FM/FE heterostructures with different types of FE substrates.

For the typical FM materials grown on PMN-PT, the magnetization versus electric field ( $M$ - $E$  curves) can be butterfly-like, loop-like, or a combination of butterfly-like and loop-like, as shown in **Figure S1**, totally depending on the composition and domain orientation of PMN-PT single crystal [1,2]. The change of magnetization behaves volatile for the butterfly-like case (**Figure S1a**), and completely vanishes when the driving electric field is removed. In contrast, nonvolatile magnetization has been demonstrated for the other two cases owing to the strain memory effect. The change of magnetization can be entirely remained for the loop-like (**Figure**

**S1b)** and partially remained for the partial-loop-like case (**Figure S1c**), where the strain memory effect commonly originates from  $109^\circ$  or  $71^\circ$  domain switching for [001] or [011] poled PMN-PT substrates, respectively [3,4]. However, the produced strains, particularly for the compressive strain, in these processes are usually small,  $-0.05\%$ . A large strain memory effect (up  $-0.45\%$ ) and nonvolatile control of magnetization can be created by utilizing the rhombohedral-to-orthorhombic (R-O) phase transformation for the [011]-poled PMN-PT substrate with composition near the morphotropic phase boundary (MPB) [5].

## **S2. Repeated measurements of isothermal $M$ - $H$ curves for the FeRh thin films grown on (011)-cut PMN-PT substrate**

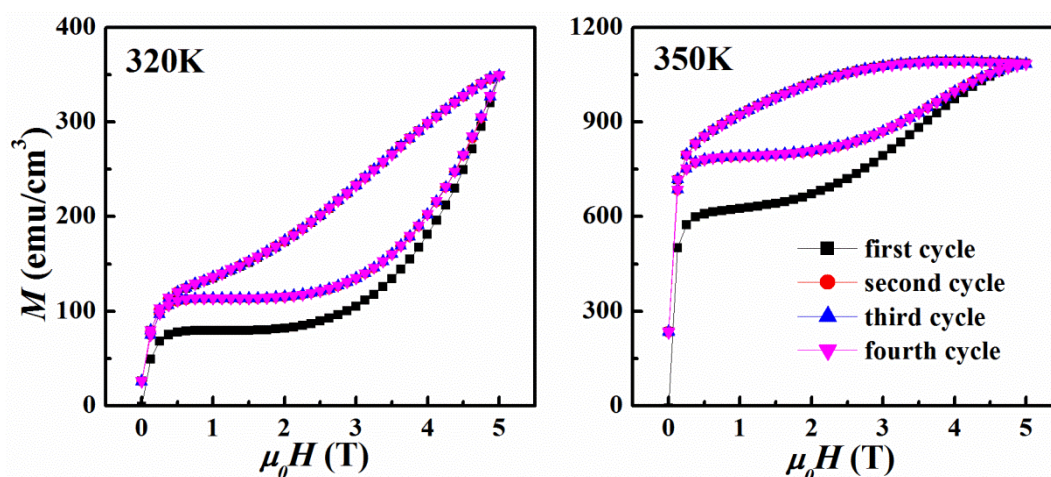


**Figure S2.** Isothermal  $M$ - $H$  curves of four continuous cycles in the absence of electric field at 320K and 350K for the FeRh/PMN-PT.

Generally, there is a degradation of magnetocaloric effect (MCE) between the virgin and following cycles for FeRh, which limits the reproducibility of the MCE. Fortunately, the measured magnetization versus magnetic field ( $M$ - $H$  curves) stays the same after the virgin cycle. The isothermal  $M$ - $H$  curves of four continuous cycles at two typical temperatures 320 K and 350 K were shown in **Figure S2**. Before the measurements at each temperature, FeRh film was cooled down to 100 K to ensure the sample at AFM phase, and then heated to the target temperature without magnetic field and electric field. Then the repeated measurements of  $M$ - $H$

curves were carried out at 320 K and 350 K. From **Figure S2**, one can notice that there indeed is a difference between the first and subsequent cycles due to virgin effect, but the  $M$ - $H$  curves stay the same after the virgin cycle.

### S3. Magnetic entropy change of FeRh film grown on PMN-PT substrate measured in loop mode

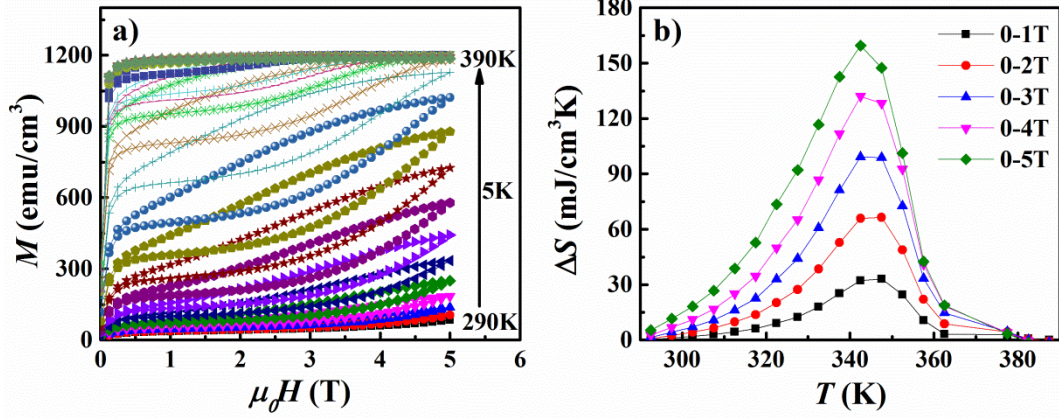


**Figure S3.** (a) Magnetization isotherms in the second cycle measured using the loop method for FeRh films. (b) Temperature dependence of magnetic entropy change computed from the isotherms.

To evaluate refrigeration capacity (RC) of FeRh film, magnetic entropy change  $\Delta S$  was calculated based on the  $M$ - $H$  data in the branch with  $H$  increasing. Note that the  $M$ - $H$  curves on  $H$  increasing remains nearly unchanged for the cases with and without the pulse  $\pm E$  (see **Figure 3c** and **d**, the path 5 almost coincides with path 3). To ensure the reliable evaluation of  $\Delta S$ , the well accepted loop method was used during the  $M$ - $H$  measurements [6]. The FeRh film was cooled down to 100 K before the  $M$ - $H$  measurements at each temperature, and second-round data were adopted to avoid virgin effect, as shown in **Figure S3a**. The magnetic entropy change  $\Delta S$  was then calculated by using Maxwell relation, as shown in **Figure S3b**. One can note that the  $\Delta S$  peaks at 343 K with a maximal value about 160 mJ cm<sup>-3</sup> K<sup>-1</sup>.

### S4. Finite element simulation of heat transfer

The heat exchange between thin films and substrates is inevitable. However, advanced means can be put forward to solve this problem during refrigeration cycling. For example, if

suitable materials can be chosen as heat transfer medium, the problem of heat leakage through substrate can be solved through careful designing the devices.

Finite element simulation is performed by taking Cu, Ag, Au, graphene, Pt as heat transfer medium, respectively, by using the Heat Transfer in Solids module of COMSOL Multiphysics 5.3.A. The details are as follows.

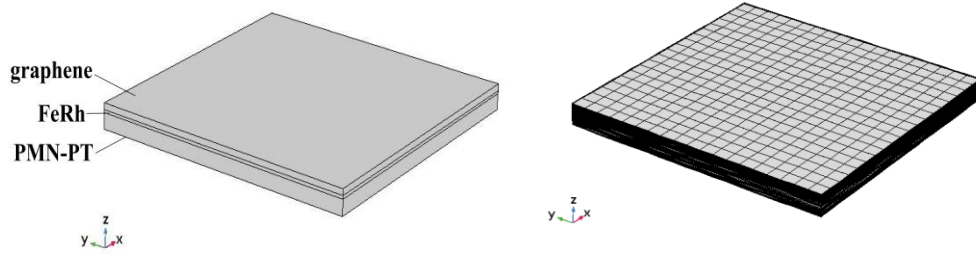


**Figure S4** (a) the simulation geometry and (b) the mesh model divided by scan mesh division method

The simulation geometry consists of 3 layers stacking, i.e. a layer acting as heat transfer medium at the top, a FeRh film at the middle, and a PMN-PT substrate at the bottom, as shown in **Figure S4**.

**Table S1** Cu, Ag, Au, graphene, Pt serving as the heat transfer medium during the simulation, respectively. Dimension, thermal conductivity ( $\kappa$ ), density ( $\rho$ ), heat capacity (C) of Cu, Ag, Au, graphene, Pt, FeRh, and PMN-PT. The simulated heat ratio  $Q_{HM}/Q_{FeRh}$  ( $Q_{HM}$  and  $Q_{FeRh}$  denote the released heat from heat medium and absorbed heat of FeRh, respectively.)

Materials	Dimension / $\mu\text{m}$	Thermal conductivity( $\kappa$ ) / $\text{Wm}^{-1}\text{K}^{-1}$	Heat capacity(C) / $\text{Jkg}^{-1}\text{K}^{-1}$	Density( $\rho$ ) / $\text{gcm}^{-3}$	$Q_{HM}/Q_{FeRh}$
Cu <sup>[7]</sup>	100×100×2	401	386	8.9	99.2%
Ag <sup>[7]</sup>	100×100×2	420	233	10.5	99.4%
Au <sup>[7]</sup>	100×100×2	318	126	19.32	98.0%
graphene	100×100×2	5000 <sup>[8]</sup>	710 <sup>[9]</sup>	2.2	97.6%
Pt <sup>[7]</sup>	100×100×2	70	135	21.45	96.6%
FeRh	100×100×1	50 <sup>[10]</sup>	360 <sup>[11]</sup>	9.76 <sup>[12]</sup>	/
PMN-PT	100×100×5	1.3 <sup>[13]</sup>	840 <sup>[14]</sup>	8.1 <sup>[13]</sup>	/

To avoid the boundary/size effect limited in finite element simulation, the thickness of FeRh is set as 1  $\mu\text{m}$ , while the length and width are both set as 100  $\mu\text{m}$ , i.e. the dimension is  $100\times 100\times 1\ \mu\text{m}^3$  for the FeRh film, which can meet the shape requirement of FeRh thin film while save the computational cost (our preliminary simulation verifies that the simple enlargement of length and width does not affect the simulated result if the thickness is fixed at 1  $\mu\text{m}$ ). Accordingly, the dimension of graphene and PMN-PT layers are set as  $100\times 100\times 2\ \mu\text{m}^3$  and  $100\times 100\times 5\ \mu\text{m}^3$ , respectively. For Cu, Ag, Au, graphene, Pt, FeRh, and PMN-PT, the parameter details of thermal conductivity ( $\kappa$ ), density ( $\rho$ ), and heat capacity (C) are presented in **Table S1**.

For the thermal resistance at interface between heat medium and FeRh or between FeRh and PMN-PT layers, the same method is adopted, i.e. averaging the  $\kappa$ ,  $\rho$ , C parameters of the upper and lower layers.

Transient analysis was performed in this calculation. The time step size is variable in order to improve calculation efficiency and meet the need of calculation accuracy. The full-coupled direct solver in Comsol software was used and the Newton method was adopted in the nonlinear iterative process. The tolerance was set as 0.01.

The model was divided into 18050 hexahedral elements by adopting scan mesh division method. The initial temperature of the heat medium and PMN-PT layers is set the same, i.e. 300K, while the initial temperature of FeRh layer is set as 291.5K to simulate the heat transfer among three layers. The whole model is considered to be an isolated system, which has no heat transfer with surroundings.

From the simulation, the evolution of temperature with time can be obtained for the 3 layers. The result is shown in **Figure S5**. Here, we assume that the temperature distribution in heat medium and FeRh film is approximately uniform due to the large thermal conductivity and smaller thickness, but the temperature distribution in PMN-PT is not uniform and the

temperature is averaged. It can be seen that Cu, Ag, Au, graphene, Pt serving as the heat transfer medium show similar rules. The temperature of heat medium sharply decreases and FeRh layer increases, while the temperature of PMN-PT layer keeps almost unchanged at the very beginning. A little time later, the temperature of heat medium and FeRh reaches equilibrium, where the heat medium reaches the minimum temperature. As time goes on, the temperature of both heat medium and FeRh increases simultaneously, while the temperature of PMN-PT decreases.

The equilibrium temperature can be obtained from **Figure S5**, which is 297.14K, 296.46K, 296.47K, 295.55K, 296.86K for Cu, Ag, Au, graphene, Pt serving as heat transfer medium, respectively. At such equilibrium temperature, heat medium reaches the minimum temperature, and the transferred heat from FeRh to heat medium (HM) reaches the maximum, which can be calculated according to the formula  $Q=Cm\Delta T$ .

$$Q_{HM} = C_{HM} m_{HM} \Delta T = C_{HM} \rho_{HM} V_{HM} (T_{HM} - T_{equil})$$

$$Q_{FeRh} = C_{FeRh} m_{FeRh} \Delta T = C_{FeRh} \rho_{FeRh} V_{FeRh} (T_{equil} - T_{FeRh})$$

where  $T_{HM}$  and  $T_{FeRh}$  denote the initial temperature of heat medium and FeRh, respectively,  $T_{equil}$  is the equilibrium temperature of heat medium and FeRh.

The heat absorbed in FeRh films equals the heat released from heat medium and PMN-PT, so the  $Q_{PMN-PT}$  can be calculated by  $Q_{PMN-PT}=Q_{FeRh}-Q_{HM}$ , where  $Q_{FeRh}$ ,  $Q_{HM}$ , and  $Q_{PMN-PT}$  denote the absorbed heat of FeRh, released heat from heat medium and PMT-PT, respectively. Therefore,

$$\frac{Q_{Cu}}{Q_{FeRh}} = 99.2\%, \quad \frac{Q_{Ag}}{Q_{FeRh}} = 99.4\%, \quad \frac{Q_{Au}}{Q_{FeRh}} = 98.0\%, \quad \frac{Q_{graphene}}{Q_{FeRh}} = 97.6\%, \quad \frac{Q_{Pt}}{Q_{FeRh}} = 96.6\%,$$

then the corresponding  $\frac{Q_{PMN-PT}}{Q_{FeRh}}$  equals 0.8%, 0.6%, 2.0%, 2.4%, 3.4% for Cu, Ag, Au,

graphene, Pt as heat medium, respectively.

From these simulation results, we find that either Cu or Ag serving as heat medium would be better than graphene, noting that the heat ratio  $Q_{\text{Cu}}/Q_{\text{FeRh}}$  (99.2%) or  $Q_{\text{Ag}}/Q_{\text{FeRh}}$  (99.4%) for the heat medium and FeRh are both larger than  $Q_{\text{graphene}}/Q_{\text{FeRh}}$  (97.6%). Moreover, Cu is readily available compared to graphene and others. **Figure S6a** shows the evolution of temperature with time by colors for the 3 layers from the view of cross section by taking Cu as the heat medium. One can notice the rapid change of temperature for the top two layers (Cu and FeRh), while the bottom layer keeps nearly unchanged before the top two reach equilibrium at  $T=297.14\text{K}$ .

Taking Cu as the heat medium, calculations indicate that the released heat to the FeRh layer by Cu accounts for 99.2%, and only 0.8% is dissipated in the PMN-PT layer at the optimal point, as shown in **Figure S6b**. So we conclude that if Cu is chosen as heat transfer medium, the problem of heat leakage through substrate can be solved, and the tiny heat leakage through substrate does not affect the cooling performance so much in an ideal cycle.

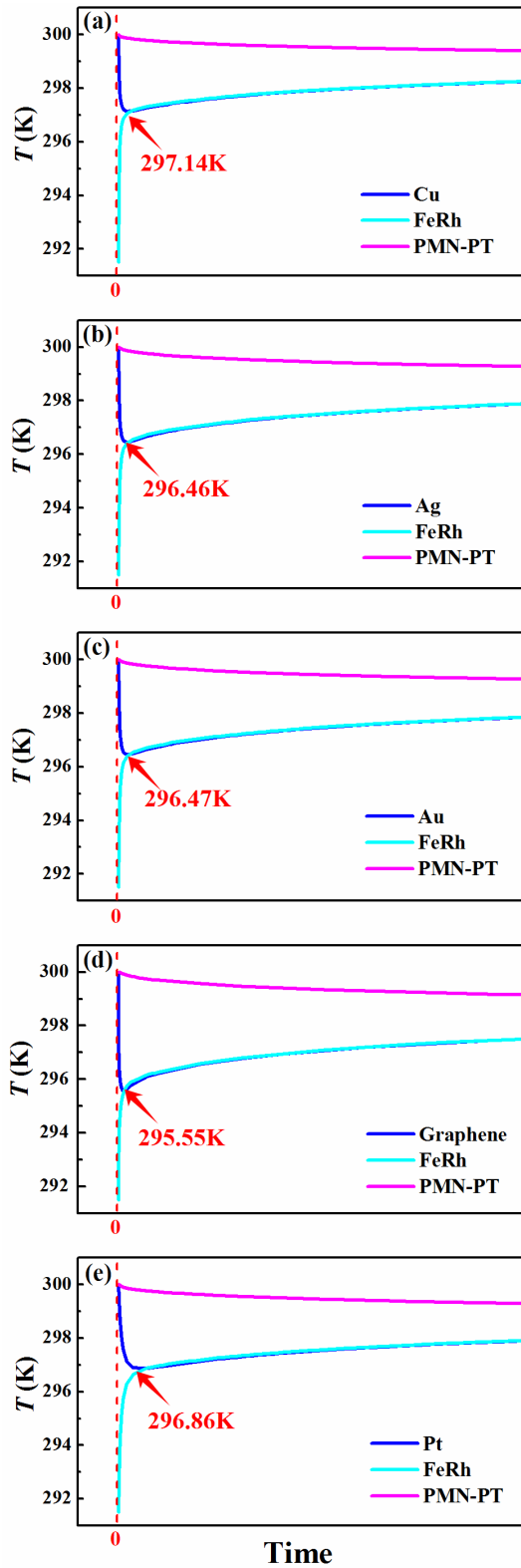


**Figure S5** Temperature evolution with time for the 3 layers composed of heat transfer medium, FeRh, and PMN-PT based on finite element simulation, where (a) Cu, (b) Ag, (c) Au, (d) graphene, (e) Pt serving as the heat transfer medium, respectively.

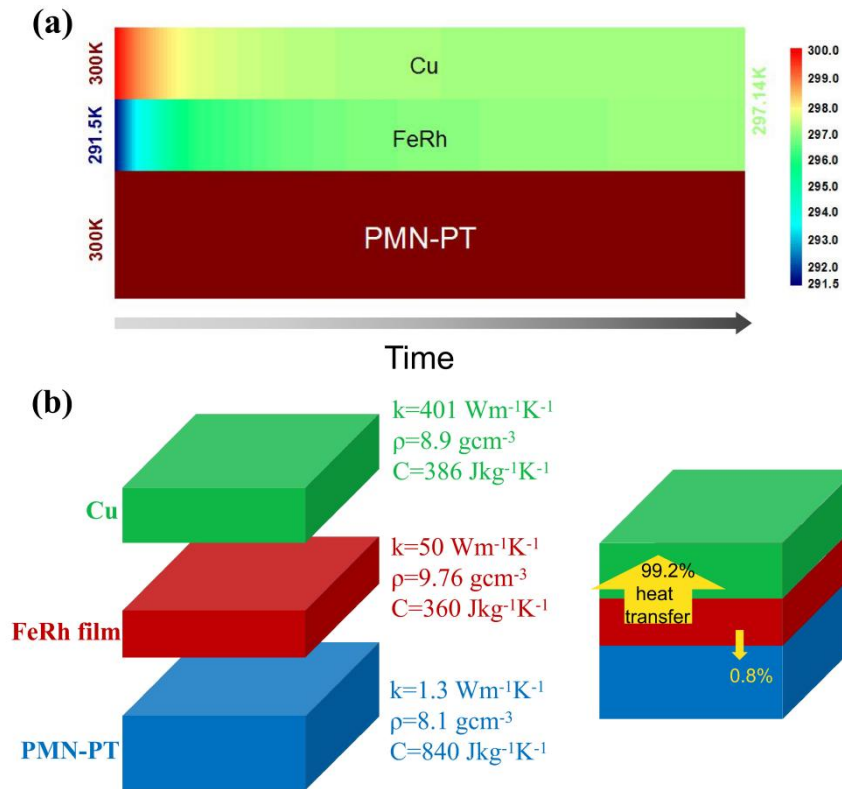


**Figure S6** Taking Cu as the heat medium, (a) temperature evolution with time indicated by colors for the 3 layers of Cu, FeRh, and PMT-PT based on finite element simulation. (b) Schematic diagram of heat transfer from FeRh film to the heat medium (Cu) and the PMN-PT substrates.

Moreover, to verify the negligible effect of the PMN-PT substrate on the magneocaloric effect of FeRh film when Cu serves as a heat transfer medium, we imitate the multilayers by making a sandwich structure composed of Cu, FeRh, and PMN-PT using conductive silver paste (thermal conductivity  $25.8\text{W/mK}$ ). Note that the produced heat in the  $50\text{nm}$  thick FeRh film is too small to be detected. In the sandwich, a  $40\mu\text{m}$  thick FeRh slice locates in the middle, a  $10\mu\text{m}$  thick Cu film acting heat transfer medium on the top, and a  $0.2\text{mm}$  thick PMN-PT substrate at the bottom. To detect the temperature, a Pt resistance is pasted on the top surface, and a resistance heater is pasted on the bottom side so as to adjust the sample to be transition temperature region by tuning electric current.

By manually moving the sample rapidly into and out of a permanent magnet ( $2\text{T}$ ) to produce magnetocaloric effect. By real-time monitoring the Pt resistance on sample by Labview

program (every 0.01s record a data point) to detect adiabatic temperature change  $\Delta T$ . **Figure S7** displays the  $\Delta T$  detected around the transition temperature (360 K) for different cases. Each pulse of  $\Delta T$  corresponds one process of sample moving in and out of the magnet by hand. For the combined PMN-PT substrate and FeRh slice without Cu at the top (**Figure S7a**, right hand),  $\Delta T$  is about 3.3K in average under a magnetic field change of 0-2.0T. When the Cu film as heat transfer medium is introduced to be on the top, the  $\Delta T$  reduces to be 2.7K because the Cu divides heat from the FeRh (**Figure S7b**, right hand). As the PMN-PT substrate is removed and only FeRh and Cu remain, the  $\Delta T$  keeps nearly unchanged, still 2.7K (**Figure S7c**, right hand), indicating that the leakage heat through the substrate is neglectable owing to the rapid process of producing and detecting heat. This result agrees well with the results of finite element simulation described above.

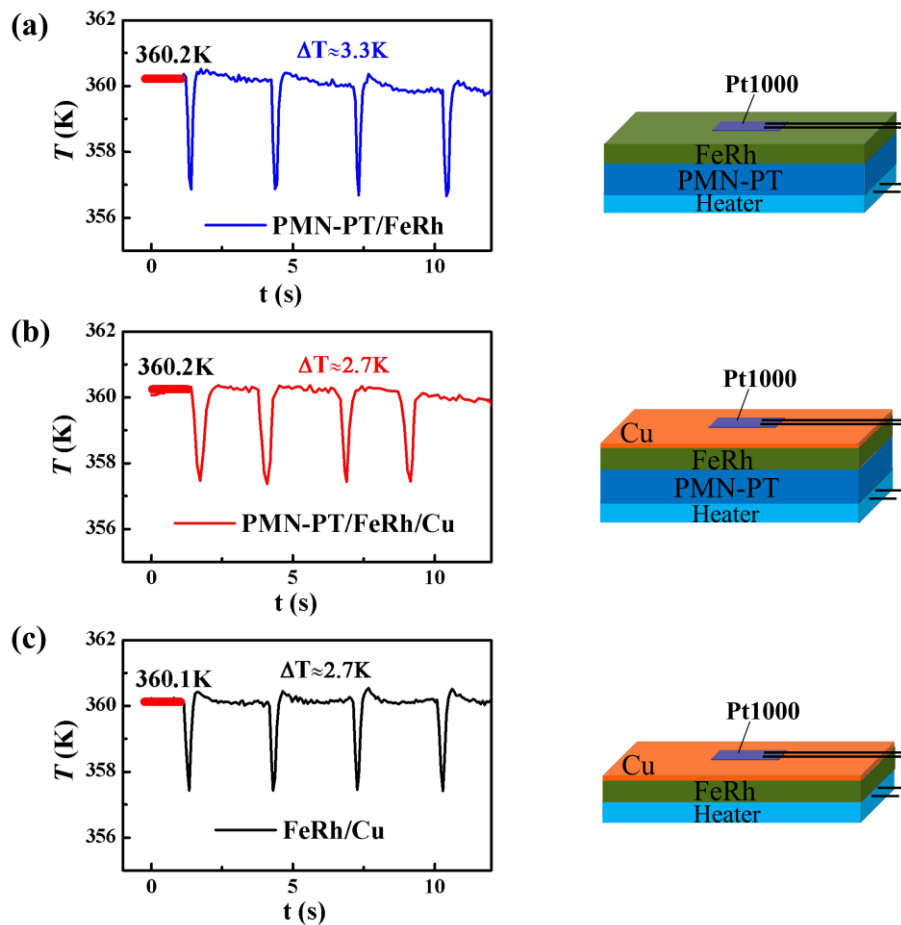


**Figure S7** The  $\Delta T$  detected around the transition temperature (360 K) for (a) PMN-PT/FeRh, (b) PMN-PT/FeRh/Cu, (c) FeRh/Cu. Each pulse represents one process of sample moving in and out of the magnet by hand. The sketches on the right present the corresponding multilayer structures during the test.

**Figure S8** displays the comparison of  $\Delta T$  as a function of temperature for these 3 cases, where the dots denote the measured data while the lines guide eyes. One can notice the clear difference in the entire phase transition region between PMN-PT/FeRh and PMN-PT/FeRh/Cu owing to the heat diversion by Cu, and the near consistency between PMN-PT/FeRh/Cu and FeRh/Cu due to the neglectable heat leakage through substrate. The discrete measurement points of  $\Delta T$  should be mainly relative to the inconsistency of manual velocity in moving the sample into and out of the magnet at each time.

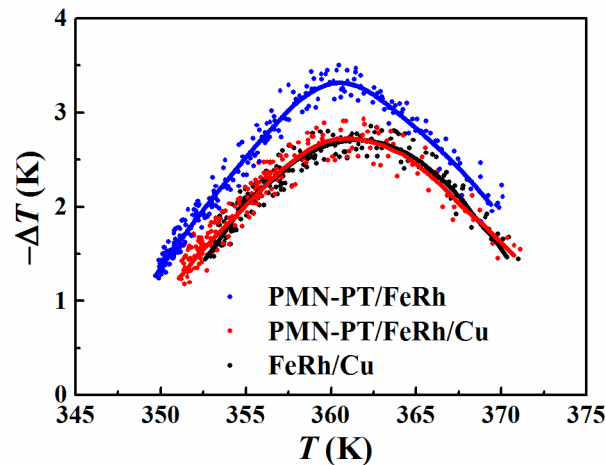


**Figure S8** The comparison of  $\Delta T$  as a function of temperature for the cases of PMN-PT/FeRh, PMN-PT/FeRh/Cu, and FeRh/Cu, where the dots denote the measured data while the lines guide eyes.

In conclusion, our experiments indicate that the leakage heat by the substrate can be neglectable if the process of producing and detecting heat can be rapid enough, where Cu film is chosen as the heat transfer medium, which takes heat from FeRh. All these agree well with the finite element simulation shown above.

## Reference

- [1] Han J. P., Cao W. W., Electric field effects on the phase transitions in [001]-oriented  $(1-x)\text{Pb}(\text{Mg}_{1/3}\text{Nb}_{2/3})\text{O}_3-x\text{PbTiO}_3$  single crystals with compositions near the morphotropic phase boundary. *Phys. Rev. B.* 68 (2003) 134102.
- [2] Liu, Y. et al. Electric-field control of magnetism in  $\text{Co}_{40}\text{Fe}_{40}\text{B}_{20}/(1-x)\text{Pb}(\text{Mg}_{1/3}\text{Nb}_{2/3})\text{O}_3-x\text{PbTiO}_3$  multiferroic heterostructures with different ferroelectric phases. *ACS Appl. Mater. Interfaces* 8 (2016) 3784–3791.
- [3] Zhang, S. et al. Electric-field control of nonvolatile magnetization in  $\text{Co}_{40}\text{Fe}_{40}\text{B}_{20}/\text{Pb}(\text{Mg}_{1/3}\text{Nb}_{2/3})_{0.7}\text{Ti}_{0.3}\text{O}_3$  structure at room temperature. *Phys. Rev. Lett.* 108 (2012) 137203.
- [4] Liu, M. et al. Voltage-Impulse-Induced Non-Volatile Ferroelastic Switching of Ferromagnetic Resonance for Reconfigurable Magnetoelectric Microwave Devices. *Adv. Mater.* 25 (2013) 4886–4892.
- [5] Shanthi M., Lim L. C., Electric-field and stress-induced R-O phase transformation in [011]-poled  $\text{Pb}(\text{Mg}_{1/3}\text{Nb}_{2/3})\text{O}_3-(28-32)\%\text{PbTiO}_3$  single crystals of [100]-length cut. *J. Appl. Phys.* 106 (2009) 114116.
- [6] Caron, L. et al. On the determination of the magnetic entropy change in materials with first-order transitions. *J. Magn. Magn. Mater.* 321 (2009) 3559–3566.
- [7] Matthias Neubronner, Thomas Bodmer, VDI Heat Atlas D6.1 Thermodynamic Properties of Pure Metals and Metal Alloys.
- [8] Alexander A. Balandin et al, Superior Thermal Conductivity of Single-Layer Graphene. *Nano Lett.*, 8 (2008) 902-907.
- [9] Eric Pop et al, Thermal properties of graphene: Fundamentals and applications. *MRS Bull.* 37 (2012) 1273.
- [10] Z. J. Ma et al, The effect of vermicularity on the thermal conductivity of vermicular graphite cast iron. *Materials and Design* 93 (2016) 418-422.
- [11] Y. Liu, Lee C. Phillips, R. Mattana, M. Bibes, A. Barthelemy, B. Dkhil, Large reversible caloric effect in FeRh thin films via a dual-stimulus multicaloric cycle. *Nat. Comm.* 7 (2016) 11614.
- [12] Chirkova et al, Giant adiabatic temperature change in FeRh alloys evidenced by direct measurements under cyclic conditions. *Acta Materialia* 106 (2016) 15-21.
- [13] Makoto Tachibana et al, Thermal conductivity and heat capacity of the relaxor ferroelectric  $[\text{PbMg}_{1/3}\text{Nb}_{2/3}\text{O}_3]_{1-x}[\text{PbTiO}_3]_x$ . *Phys. Rev. B* 79 (2009) 100104(R).

[14] E. W. Sun, & W. W. Cao, Relaxor-based ferroelectric single crystals: growth, domain engineering, characterization and applications. *Prog. Mater. Sci.* 65 (2014) 124–210.